

## Tunneling Spectra of Individual Magnetic Endofullerene Molecules

Jacob E. Grose,<sup>1</sup> Eugenia S. Tam,<sup>1</sup> Carsten Timm,<sup>2</sup> Michael Scheloske,<sup>3</sup> Burak Ulgut,<sup>4</sup>

Joshua J. Parks,<sup>1</sup> Héctor D. Abruña,<sup>4</sup> Wolfgang Harneit,<sup>3</sup> and D. C. Ralph<sup>1\*</sup>

<sup>1</sup>*Laboratory of Atomic and Solid State Physics, Cornell University, Ithaca, NY 14853, USA*

<sup>2</sup>*Department of Physics and Astronomy, University of Kansas, Lawrence, Kansas 66045, USA*

<sup>3</sup>*Institut für Experimentalphysik, Freie Universität Berlin, Arnimallee 14, 14195 Berlin, Germany*

<sup>4</sup>*Department of Chemistry and Chemical Biology, Cornell University, Ithaca, NY 14853, USA*

The manipulation of single magnetic molecules may enable new strategies for high-density information storage and quantum-state control. However, progress in these areas depends on developing techniques for addressing individual molecules and controlling their spin. Here we report success in making electrical contact to individual magnetic N@C<sub>60</sub> molecules and measuring spin excitations in their electron tunneling spectra. We verify that the molecules remain magnetic by observing a transition as a function of magnetic field which changes the spin quantum number and also the existence of nonequilibrium tunneling originating from low-energy excited states. From the tunneling spectra, we identify the charge and spin states of the molecule. The measured spectra can be reproduced theoretically by accounting for the exchange interaction between the nitrogen spin and electron(s) on the C<sub>60</sub> cage.

Magnetic molecules provide the opportunity to study, at a fundamental level, the origins of ferromagnetism and quantum aspects of magnetic dynamics<sup>1,2</sup>. Proposals suggest that their spin degrees of freedom could also serve as useful qubits for quantum manipulation<sup>3</sup>. Most previous experiments on magnetic molecules have examined samples consisting of many molecules; however, applications and more detailed scientific studies will require the ability to address individual molecules. Here we report the use of tunneling spectroscopy within single-molecule transistors (SMTs), a technique which has been used previously to measure vibrational and electronic excitations<sup>4-6</sup>, to achieve electrical contact to individual molecules of the spin-3/2 endohedral fullerene N@C<sub>60</sub> (Fig. 1a) and to measure its spin excitations. N@C<sub>60</sub> is an attractive model system<sup>7,8</sup> because of its simple spin structure and because of the possibility of control experiments employing nonmagnetic C<sub>60</sub> molecules<sup>4,9-13</sup>. N@C<sub>60</sub> molecules also have the advantage of being stable<sup>14</sup> at the high temperatures present during the electromigration process by which our molecular-scale junctions are formed<sup>15,16</sup>. Previous SMT experiments using less robust Mn<sub>12</sub>-based magnetic molecules detected magnetic signatures in a few samples<sup>17,18</sup>, but found that the molecular magnetism was usually destroyed during device fabrication<sup>18</sup>. We observe that the N@C<sub>60</sub> devices exhibit clear magnetic character, in that they have a spin-state transition as a function of applied magnetic field. The nature of this transition allows us to identify the charge and spin states of the molecule in the SMT. The spectra of N@C<sub>60</sub> also exhibit low energy excited states and signatures of nonequilibrium spin excitations predicted for this molecule<sup>19</sup>. We associate the existence of a spin transition in N@C<sub>60</sub> accessible at laboratory magnetic

fields with the scale of the exchange interaction between the nitrogen spin and electron(s) on the  $C_{60}$  cage.

The geometry of our SMT devices is shown in Fig. 1b. We make the devices by adsorbing the molecules onto an initially-continuous Pt wire on top of an oxidized Al gate electrode and then breaking the wire using electromigration to form a nm-scale gap. (Additional information about fabrication procedures is given in the Methods section.) We identify the presence of one or more molecules in the gap by the observation of gate-dependent Coulomb-blockade transport characteristics<sup>5,11</sup>. Our success rate for obtaining such devices was 9/19 for  $N@C_{60}$  devices and 17/59 for  $C_{60}$  devices, while 0/39 control samples prepared using pure toluene instead of a fullerene solution showed Coulomb blockade. Six of the  $N@C_{60}$  devices were sufficiently stable for detailed measurements.

The most striking difference between the  $N@C_{60}$  devices and the  $C_{60}$  controls is seen in the magnetic field dependence of the tunneling conductance spectra. In Fig. 2 we show these spectra as a function of source-drain voltage ( $V$ ) and magnetic field ( $B$ ) at dilution-refrigerator temperatures (electron temperature  $\approx 100$  mK) for values of gate voltage ( $V_g$ ) more positive than the only experimentally accessible “degeneracy point” -- the value of gate voltage for which the energy difference between the two accessible charge states is zero, so that current can flow even near  $V = 0$ . Figure 3 shows the conductance for each sample as a function of  $V$  and  $V_g$  near the degeneracy point. (By focusing on low-voltage transport near one degeneracy point, we ensure that tunneling is occurring through a single molecule<sup>5</sup>). In the  $N@C_{60}$  devices, as a function of increasing  $B$  (Fig. 2a,b) the lowest-voltage conductance peaks at positive and negative bias first move apart and then change slope to move back closer together. These initial peaks can

be associated with the same quantum transition from the ground state of one charge state (charge  $q$ ) of the molecule to the ground state with charge  $q+1$  (one fewer electron). At the value of  $B$  where the slopes of the peaks change sign in Fig. 2a, we observe level crossings, where a conductance peak that at low  $B$  is associated with an excited state of charge  $q+1$  becomes the ground state of charge  $q+1$  at high  $B$ . We measured ground-state conductance peaks that shift apart then together as a function of  $B$  on the positive-gate side of the degeneracy point in four out of five of the N@C<sub>60</sub> devices on which we performed this measurement. (The fifth showed no change in slope up to 9 T.) The field values at which the crossovers occurred varied from approximately 1 T to 7 T.

The level crossing in Fig. 2a shows that the change in sign of the ground-state-peak slopes is due to an increase in total spin component  $S_{z,q+1}$  along the magnetic field direction  $\hat{z}$  for the lowest-energy charge  $q+1$  state. The slopes of the peaks as a function of  $B$  imply that at low fields  $S_{z,q} > S_{z,q+1}$ , and at high fields  $S_{z,q} < S_{z,q+1}$ . Assuming that  $|S_{z,q+1} - S_{z,q}| = 1/2$ , the slopes of the conductance resonances vs. magnetic field shown in Fig. 2 correspond to an electronic  $g$ -factor  $|g| = 2.0 \pm 0.3$ .

In contrast, Fig. 2c shows the tunneling spectrum for a C<sub>60</sub> device also taken on the positive-gate side of its degeneracy point. Of the five C<sub>60</sub> devices we measured as a function of magnetic field, none showed a change in the sign of the slopes for the lowest-voltage tunneling transition. While the spectra for the C<sub>60</sub> devices often contain low-energy excitations in the same range of energy as those of N@C<sub>60</sub>, 0.1 meV to several meV, the lack of spin transitions suggests that the low-lying excitations in C<sub>60</sub> are vibrational<sup>4,11,20</sup>, rather than electronic or magnetic.

We assert that the spin-state transition in the N@C<sub>60</sub> devices is likely associated

with two states with different values of total spin, as opposed to two states within the same multiplet split by magnetic anisotropy. Because any magnetic anisotropy axes could be oriented arbitrarily relative to the applied magnetic field, if the transition were due to states split by magnetic anisotropy one should expect, in general, that the slopes of the energy levels as a function of  $B$  should show deviations from  $|g| = 2$  and exhibit strong deviations from linearity at low field<sup>18,21,22</sup>. In our data, any such deviations are small. The lack of observable magnetic anisotropy effects is consistent with the symmetries of  $N@C_{60}$  and the weak spin-orbit coupling of its constituent atoms<sup>23</sup>.

With this understanding, the existence of a spin-state transition at an accessible magnetic field for the charge  $q+1$  energy levels of  $N@C_{60}$  allows us to identify the charge and spin states involved in the tunneling. Consider the possible states shown in Fig. 1c, which depicts the nitrogen spin (blue arrow) coupled to electron spins (black arrows) occupying the lowest unoccupied molecular orbital (LUMO) of the  $C_{60}$ . We assume that a 3-fold degeneracy of the LUMOs of isolated  $C_{60}$  is broken by molecular deformation due to interaction with the electrodes or the Jahn-Teller effect<sup>24</sup>, and we consider only the experimentally accessible neutral and negative charge states. Neutral  $N@C_{60}$  is known to have spin  $3/2$  because the encapsulated nitrogen retains its atomic electronic configuration<sup>25</sup>. When electrons are added to  $N@C_{60}$ , they are believed to occupy the LUMO of the  $C_{60}$  molecule<sup>26</sup>. With the addition of one extra electron,  $N@C_{60}^{1-}$  may therefore have either  $S = 1$  or  $2$ , and these two multiplets are split in energy by the exchange interaction between the N spin and the electron spin. If the exchange is antiferromagnetic, the ground state will have  $S = 1$  for low  $B$  and  $S = 2$  for large  $B$ . For  $N@C_{60}^{2-}$ , the total spin should again be  $S = 3/2$  since the splitting between the LUMO

states is expected to be large compared to the Hund's rule coupling. Because we observe the spin-state transition in the *more positive* of the two charge states involved in tunneling, the 0/1- charge couple can be ruled out as the charge states between which tunneling occurs. This leads to the identification, for an antiferromagnetic exchange interaction, that 1-/2- is the couple with the lowest charge magnitude that is capable of transitioning from  $S_q - S_{q+1} = +1/2$  at low fields to  $S_q - S_{q+1} = -1/2$  at high fields. For a ferromagnetic exchange interaction, the lowest-magnitude charge couple possibly consistent with the data would be 2-/3-, which is unlikely because the 3- charge state should have a much higher energy than 1- or 2- states. A 2-/3- scenario would also require fine tuning such that the exchange splitting is approximately equal to the deformation-induced level splitting within the  $N@C_{60}^{2-}$  LUMO.

The identification of our measured spectra with the 1-/2- charge couple implies that our  $N@C_{60}$  devices are in the 2- charge state at  $V_g = 0$ , which may seem to be a large magnitude of charge in an unbiased device. However, for  $C_{60}$  in the gas phase, both the 1- and 2- states are more stable than the neutral form, with the 2- state quite close in energy to the 1- state<sup>27-29</sup>. The equilibrium charge of  $C_{60}$  is generally found to be either 1- or 2- when it is adsorbed on noble metal surfaces<sup>30,31</sup>. These previous studies suggest that the 3- charge state is likely to have a much higher energy than 1- or 2- in an unbiased device, which argues against the possibility of a ferromagnetic exchange interaction in our samples as this would require a 2-/3- charge couple with a 3- charge state at zero gate voltage. In regard to the sign of the exchange interaction, an *ab-initio* calculation has predicted a weakly ferromagnetic interaction in  $N@C_{60}^{1-}$ , rather than the antiferromagnetic interaction we suggest<sup>32</sup>. However, it should be noted that the

calculation of the exchange interaction is difficult since it is computed as a small difference between large total energies.

The device-to-device variations that we measure in the N@C<sub>60</sub> tunneling spectra indicate that the energies of the electronic states are perturbed differently by the environment in each device. In order to explain the variations in field value giving rise to the spin-state transition, the strength of the exchange interaction must differ between devices, presumably due to different amounts of molecular deformation and/or local electric fields. If we parameterize the exchange interaction in the form  $J\mathbf{s}_e \cdot \mathbf{S}_N$ , where  $\mathbf{s}_e$  is the total electron spin and  $\mathbf{S}_N$  is the spin on the nitrogen atom, then measured transition fields (1 to 7 T) imply exchange strengths,  $|J|$ , between 0.06 meV and 0.4 meV.

To understand how the measured tunneling spectra might relate to the molecular magnetism, we have calculated the conductance of an N@C<sub>60</sub> transistor (Fig. 4a,b). As a minimal model to account for the low-energy transitions, we consider the energy level diagrams shown in Fig. 4c,d, which include the three multiplets, ( $q = -2, S = 3/2$ ), ( $q = -1, S = 1$ ), and ( $q = -1, S = 2$ ), we have introduced previously and also the lowest-energy excited-state multiplet associated with each of these states. The excited multiplets could correspond to the added excitation of a long-lived vibrational mode or energy shifts due to charging in nearby molecules. We assume that the molecule has negligible magnetic anisotropy, so that all of the magnetic effects we consider are due to exchange-induced level splittings. This is in contrast to previous calculations for Mn<sub>12</sub>-type molecules where the low-energy spectra were assumed to be dominated by large magnetic anisotropy<sup>17,18</sup>. We use the rate-equation approach<sup>19</sup> to calculate the differential

conductance. Parameter values, listed in the Methods section, are selected to approximate the data in Fig. 2a and 3a.

There are a sufficiently large number of free parameters that we do not seek or claim quantitative agreement. Depending on assumptions about the value of  $J$  and vibrational parameters, different numbers of excited-state tunneling transitions are possible. Nevertheless the calculation can reproduce many of the qualitative features seen in Fig. 2 and 3. First, the N@C<sub>60</sub> spectra shown in Fig. 3a,b and the theoretical results shown in Fig. 4b both exhibit a consequence of nonequilibrium excitations that was predicted previously<sup>19</sup>. If one extrapolates the conductance peaks marked by yellow triangles in Fig. 3a and b toward zero voltage, they do not extend all the way to the line corresponding to the ground-state tunneling threshold, but instead terminate when they intersect a conductance peak corresponding to an excited-state transition. We observed this type of feature in four of six N@C<sub>60</sub> devices, but in none of thirteen C<sub>60</sub> devices that were stable enough for detailed study (*e.g.*, Fig. 3c). Elste and Timm explain this phenomenon in terms of excited-state-to-excited-state (ETE) transitions<sup>19</sup>. The idea is illustrated by Fig. 4c,d. Here ground-state tunneling at low magnetic field corresponds to the transition (labeled A) from the  $q = -2, S = 3/2$  state to  $q = -1, S = 1$ . For a sufficiently large applied voltage  $V$ , the tunneling of an electron back into the molecule can lead to a transition (labeled b) from the  $q = -1, S = 1$  state to the excited  $q = -2, S = 3/2$  multiplet, rather than the ground state  $S = 3/2$  multiplet. If this excited state does not relax before the next electron tunnels out of the molecule, this will produce an ETE conductance peak corresponding to a transition (B) between the excited  $q = -2, S = 3/2$  multiplet and the excited  $q = -1, S = 2$  multiplet. The reason that transition B cannot extrapolate

indefinitely to lower voltage is that the applied bias must provide sufficient energy to permit the transition b for transition B to be possible. As support for this interpretation, note that the level diagram in Fig. 4c,d requires that  $E_C = E_B + (E_b - E_a)$ . Using the measured values of the excitation energies (see the caption for Fig. 3), this equality is satisfied within experimental uncertainty.

Another successful feature of the calculation is that it can account for the magnetic-field dependence of the tunneling spectrum shown in Fig. 2a. In particular, note that this spectrum has two conductance peaks that as a function of magnetic field intersect the lowest-voltage transition but then terminate so that they do not produce a level crossing—this happens near 1.5 T for transition B and 4 T for transition C. Only near 7 T is there a true level crossing for transition D that corresponds to the spin-state transition discussed above. The “non-crossing” levels can be understood as another consequence of nonequilibrium ETE transitions. For voltages less than the ground-state to ground-state transition, the first electron tunneling event that initiates current flow is not allowed, so that the excited states cannot be populated.

One difference between the calculated spectrum in Fig. 4a,b and the measurements in Fig. 2a and 3a is that the calculated spectrum contains two more lines at positive bias (7 lines at  $B = 0$  instead of 5). The extra lines correspond to non-equilibrium ETE transitions from the excited  $q = -2, S = 3/2$  state to the two  $q = -1, S = 2$  states (i.e., they are lower-energy satellites of transitions D and E.) We suspect that these extra transitions are present but unresolved in the experimental spectra because the linewidths of the experimental transitions increase as a function of energy and the ETE

transitions have weaker amplitudes than transitions originating from the ground state, thereby making them difficult to distinguish at higher energies.

The capability to make electrical contact to single magnetic molecules without destroying their magnetic character provides the foundation for more advanced strategies to manipulate spin states. We have shown that the charge and spin values of the molecule can be identified, that spin excitation energies can be measured, and that the tunneling spectrum of N@C<sub>60</sub> can be understood qualitatively within an elementary model. The next challenges will include developing the means to coherently populate desired superpositions of spin states (using, for instance, applied microwaves<sup>3,33</sup> or electrical manipulation<sup>34</sup>), developing accurate techniques to read out spin information, and achieving improved control over the interaction between the magnetic molecule and its environment so as to minimize device-to-device variations.

## **METHODS**

**Synthesis:** N@C<sub>60</sub> was synthesized by continuous nitrogen ion implantation into freshly sublimed fullerene layers<sup>25</sup> with a yield (N@C<sub>60</sub>:C<sub>60</sub> ratio) of  $\sim 10^{-4}$ . The N@C<sub>60</sub> contained in the harvested product was enriched and purified by multi-step high-pressure liquid chromatography (HPLC)<sup>35</sup>. Purity was checked by UV-Vis absorption, HPLC, and electron spin resonance and found to be better than 99.5%.

**Electrochemistry:** We have confirmed, using electrochemical measurements, that the interaction in N@C<sub>60</sub> between the N atom and the extra electrons on C<sub>60</sub> is relatively

weak. Cyclic voltammograms were performed on N@C<sub>60</sub> or C<sub>60</sub> films formed by drop casting from toluene solutions onto a 3 mm Pt disc electrode, polished to a mirror finish, used as the working electrode. A Ag/AgCl (saturated NaCl) and a Pt coil were used as the reference and counter electrodes, respectively. The scans, carried out at a sweep rate of 500 mV/s, were done in 0.1 M tetrabutylammonium hexafluorophosphate in acetonitrile in a single-compartment cell. The solution was deoxygenated via N<sub>2</sub> bubbling for 10 min before the sweeps, which were run in a N<sub>2</sub> atmosphere. We found that the first two reductions of N@C<sub>60</sub> occur within 25 mV of those of C<sub>60</sub>. The ~25 mV shifts are not related to the nature of the molecules and can be attributed to the varying rates of dissolution of the reduced species due to slight variations in the film morphology. This arises as a result of the fact that while the neutral forms of C<sub>60</sub> and N@C<sub>60</sub> are insoluble in acetonitrile, the reduced forms are not.

**Sample Fabrication:** Our single-molecule transistors were fabricated following a procedure similar to those used previously<sup>4,5</sup>. First we made an Al gate electrode 16 nm thick and 2 μm wide on an oxidized Si wafer, and exposed the Al to air to form a thin insulating oxide. On top of the gate electrode, we fabricated continuous Pt wires with widths of approximately 150 nm and thicknesses of 10 nm. The chips were cleaned with an oxygen plasma and immediately covered with 25 μL of either a 0.1 mM solution of N@C<sub>60</sub> for 2.5 minutes or (for one type of control sample) a 0.5 mM solution of C<sub>60</sub> in toluene for 1 minute. Then the excess solution was blown off the chip, and the deposition process was repeated. We found that repeating the deposition process produced a more convenient yield of single-molecule devices. After the molecules were deposited, we

cooled to cryogenic temperatures and broke the wires using electromigration in a circuit with small series resistance<sup>16</sup>, thereby forming nm-scale gaps in which a molecule was sometimes trapped. The breaking voltages for our Pt wires were in the range 1-1.5 V.

**Low-temperature measurements:** The measurements were performed in a dilution refrigerator equipped with room-temperature low-pass filters and low-temperature copper powder filters on all electrical lines. The electron temperature calibrated on quantum dot samples is  $< 100$  mK.

**Theory:** The differential conductance  $dI/dV$  is calculated using the rate-equation approach in the sequential-tunneling approximation<sup>19</sup>. The electronic molecular Hamiltonian reads

$$H_{\text{el}} = (\varepsilon - eV_g^*) \sum_{\sigma} a_{\sigma}^{\dagger} a_{\sigma} + U a_{\uparrow}^{\dagger} a_{\uparrow} a_{\downarrow}^{\dagger} a_{\downarrow} - J \mathbf{s}_e \cdot \mathbf{S}_N - B (S_e^z + S_N^z) \quad (\text{S1})$$

where  $\varepsilon$  is the on-site energy of electrons with spin  $\sigma = \uparrow, \downarrow$  created by  $a_{\sigma}^{\dagger}$ ,  $V_g^*$  is the electric potential at the position of the molecule,  $U$  is the Coulomb repulsion,  $J$  is the exchange interaction between the nitrogen spin  $\mathbf{S}_N$  and the spin  $\mathbf{s}_e = \sum_{\sigma\sigma'} a_{\sigma}^{\dagger} (\boldsymbol{\sigma}_{\sigma\sigma'} / 2) a_{\sigma'}$  of the electrons in the LUMO, and  $B$  is the magnetic field with a factor  $g\mu_B$  absorbed. Only one LUMO is included, the other two are assumed to be split off due to molecular deformation and to not to affect  $dI/dV$ . The asymmetric contact capacitances and the fact that the bias voltage is applied to the (arbitrarily labeled) left electrode are incorporated by writing  $V_g^* = \alpha V_g + \beta_L V$  with the applied gate voltage  $V_g$  and bias voltage  $V$ , where  $\alpha = 0.15$  and  $\beta_L = 0.25$  give the best fit. Asymmetric tunneling amplitudes  $t_{L,R}$  between

the LUMO and the left and right electrodes are assumed; a ratio  $t_L / t_R = 0.4$  is used. In addition, we include low-energy excitations of energy  $\hbar\omega_n$  in the  $n$ - charge state, which in this description for the sake of definiteness we assume to be vibrational. The transition rates between vibrational states contain Franck-Condon matrix elements<sup>36</sup>  $M_{nm,n'm'}$  (with electron numbers  $n, n'$  and oscillator quantum numbers  $m, m'$ ) with relative values of the nonvanishing components  $M_{20,10} = M_{20,11} = M_{21,11} = M_{22,10} = 1$  and  $M_{21,10} = 0.7$ ; the matrix is symmetric. The other parameters used in the calculations are  $\varepsilon = -3.23415$ ,  $U = 3.1$ ,  $J = -0.0004$ ,  $k_B T = 0.00002$  all in eV.

### Acknowledgements

We thank R. Döring and O. Bäblier for their work to synthesize and purify the N@C<sub>60</sub> and G. R. Hutchison for help with calculations. The research at Cornell was supported by the US NSF (DMR-0520404, DMR-0605742, EEC-0646547, CHE-0403806 and through use of the Cornell Nanofabrication Facility/NNIN). Work in Berlin was supported by the *Bundesministerium für Bildung und Forschung* under contract no. 03N8709.

JEG played the primary role in fabricating the samples, performing the measurements, and analyzing the data, with assistance from EST and JJP and advice from DCR. CT performed the model calculations. MS and WH led the molecular synthesis, purification, and characterization. BU and HAB performed electrochemical characterization. All of the authors contributed to the data analysis and the preparation of the manuscript.

## **Competing Interests Statement**

The authors declare that they have no competing financial interests.

## References

1. Gatteschi, D. & Sessoli, R. Quantum tunneling of magnetization and related phenomena in molecular materials. *Angew. Chem. Int. Ed.* **42**, 268-297 (2003).
2. Bogani, L. & Wernsdorfer, W. Molecular spintronics using single-molecule magnets. *Nature Mater.* **7**, 179-186 (2008).
3. Leuenberger, M. N. & Loss, D. Quantum computing in molecular magnets. *Nature* **410**, 789-793 (2001).
4. Park, H. et al. Nanomechanical oscillations in a single-C<sub>60</sub> transistor. *Nature* **407**, 57-60 (2000).
5. Park, J. et al. Coulomb blockade and the Kondo effect in single-atom transistors. *Nature* **417**, 722-725 (2002).
6. Liang, W. J., Shores, M. P., Bockrath, M., Long, J. R. & Park, H. Kondo resonance in a single-molecule transistor. *Nature* **417**, 725-729 (2002).
7. Harneit, W. Fullerene-based electron-spin quantum computer. *Phys. Rev. A* **65**, 032322 (2002).
8. Morton, J. J. L. et al. Bang-bang control of fullerene qubits using ultrafast phase gates. *Nat. Phys.* **2**, 40-43 (2006).
9. Joachim, C. & Gimzewski, J. K. An electromechanical amplifier using a single molecule. *Chem. Phys. Lett.* **265**, 353-357 (1997).
10. Lu, X. H., Grobis, M., Khoo, K. H., Louie, S. G. & Crommie, M. F. Spatially mapping the spectral density of a single C<sub>60</sub> molecule. *Phys. Rev. Lett.* **90**, 096802 (2003).

11. Yu, L. H. & Natelson, D. The Kondo effect in C<sub>60</sub> single-molecule transistors. *Nano Lett.* **4**, 79-83 (2004).
12. Pasupathy, A. N. et al. The Kondo effect in the presence of ferromagnetism. *Science* **306**, 86-89 (2004).
13. Champagne, A. R., Pasupathy, A. N. & Ralph, D. C. Mechanically-adjustable and electrically-gated single-molecule transistors. *Nano Lett.* **5**, 305-308 (2005).
14. Waiblinger, M. et al. Thermal stability of the endohedral fullerenes N@C<sub>60</sub>, N@C<sub>70</sub>, and P@C<sub>60</sub>. *Phys. Rev. B* **64**, 159901(E) (2001).
15. Trouwborst, M. L., van der Molen, S. J. & van Wees, B. J. The role of Joule heating in the formation of nanogaps by electromigration. *J. Appl. Phys.* **99**, 114316 (2006).
16. Taychatanapat, T., Bolotin, K. I., Kuemmeth, F. & Ralph, D. C. Imaging electromigration during the formation of break junctions. *Nano Lett.* **7**, 652-656 (2007).
17. Heersche, H. B. et al. Electron transport through single Mn<sub>12</sub> molecular magnets. *Phys. Rev. Lett.* **96**, 206801 (2006).
18. Jo, M.-H. et al. Signatures of molecular magnetism in single-molecule transport spectroscopy. *Nano Lett.* **6**, 2014-2020 (2006).
19. Elste, F. & Timm, C. Theory for transport through a single magnetic molecule: Endohedral N@C<sub>60</sub>. *Phys. Rev. B* **71**, 155403 (2005).
20. Pasupathy, A. N. et al. Vibration-assisted electron tunneling in C<sub>140</sub> single-molecule transistors. *Nano Lett.* **5**, 203-207 (2005).
21. Guéron, S., Deshmukh, M. M., Myers, E. B. & Ralph, D. C. Tunneling via individual electronic states in ferromagnetic nanoparticles. *Phys. Rev. Lett.* **83**, 4148-4151 (1999).

22. Timm, C. Tunneling through magnetic molecules with arbitrary angle between easy axis and magnetic field. *Phys. Rev. B* **76**, 014421 (2007).
23. Huertas-Hernando, D., Guinea, F. & Brataas, A. Spin-orbit coupling in curved graphene, fullerenes, nanotubes, and nanotube caps. *Phys. Rev. B* **74**, 155426 (2006).
24. Green, W. H. et al. Electronic structures and geometries of  $C_{60}$  anions via density functional calculations. *J. Phys. Chem.* **100**, 14892-14898 (1996).
25. Almeida Murphy, T. et al. Observation of atomlike nitrogen in nitrogen-implanted solid  $C_{60}$ . *Phys. Rev. Lett.* **77**, 1075-1078 (1996).
26. Pietzak, B., Weidinger, A., Dinse, K.-P. & Hirsch, A. in *Endofullerenes: A New Family of Carbon Clusters*, Akasaka, T. & Nagase, S., Eds. (Kluwer, Dordrecht, 2002) pp. 13-65.
27. Yang, S. H., Pettiette, C. L., Conceicao, J., Cheshnovsky, O. & Smalley, R. E. UPS of Buckminsterfullerene and other large clusters of carbon. *Chem. Phys. Lett.* **139**, 233-238 (1987).
28. Pederson, M. R. & Quong, A. A. Polarizabilities, charge states, and vibrational modes of isolated fullerene molecules. *Phys. Rev. B* **46**, 13584-13591 (1992).
29. Yannouleas, C. & Landman, U. Stabilized-jellium description of neutral and multiply charged fullerenes  $C_{60}^{x\pm}$ . *Chem. Phys. Lett.* **217**, 175 (1994).
30. Modesti, S., Cerasari, S. & Rudolf, P. Determination of charge states of  $C_{60}$  adsorbed on metal surfaces. *Phys. Rev. Lett.* **71**, 2469-2472 (1993).
31. Swami, N., He, H. & Koel, B. E. Polymerization and decomposition of  $C_{60}$  on Pt(111) surfaces. *Phys. Rev. B* **59**, 8283-8291 (1999).

32. Udvardi, L., in *Electronic Properties of Novel Materials - Molecular Nanostructures*, Kuzmany, H., Fink, J., Mehring, M. & Roth, S., Eds. (AIP, Melville, 2000) pp. 187-190.
33. Harneit, W. et al. Room temperature electrical detection of spin coherence in C<sub>60</sub>. *Phys. Rev. Lett.* **98**, 216601 (2007).
34. Nowack, K. C., Koppens, F. H. L., Nazarov, Yu. V. & Vandersypen, L. M. K. Coherent control of a single electron spin with electric fields. *Science* **318**, 1430-1433 (2007).
35. Jakes, P., Dinse, K.-P., Meyer, C., Harneit, W. & Weidinger, A. Purification and optical spectroscopy of N@C<sub>60</sub>. *Phys. Chem. Chem. Phys.* **5**, 4080-4083 (2003).
36. Koch, J., von Oppen, F., Oreg, Y. & Sela, E. Thermopower of single-molecule devices. *Phys. Rev. B* **70**, 195107 (2004).

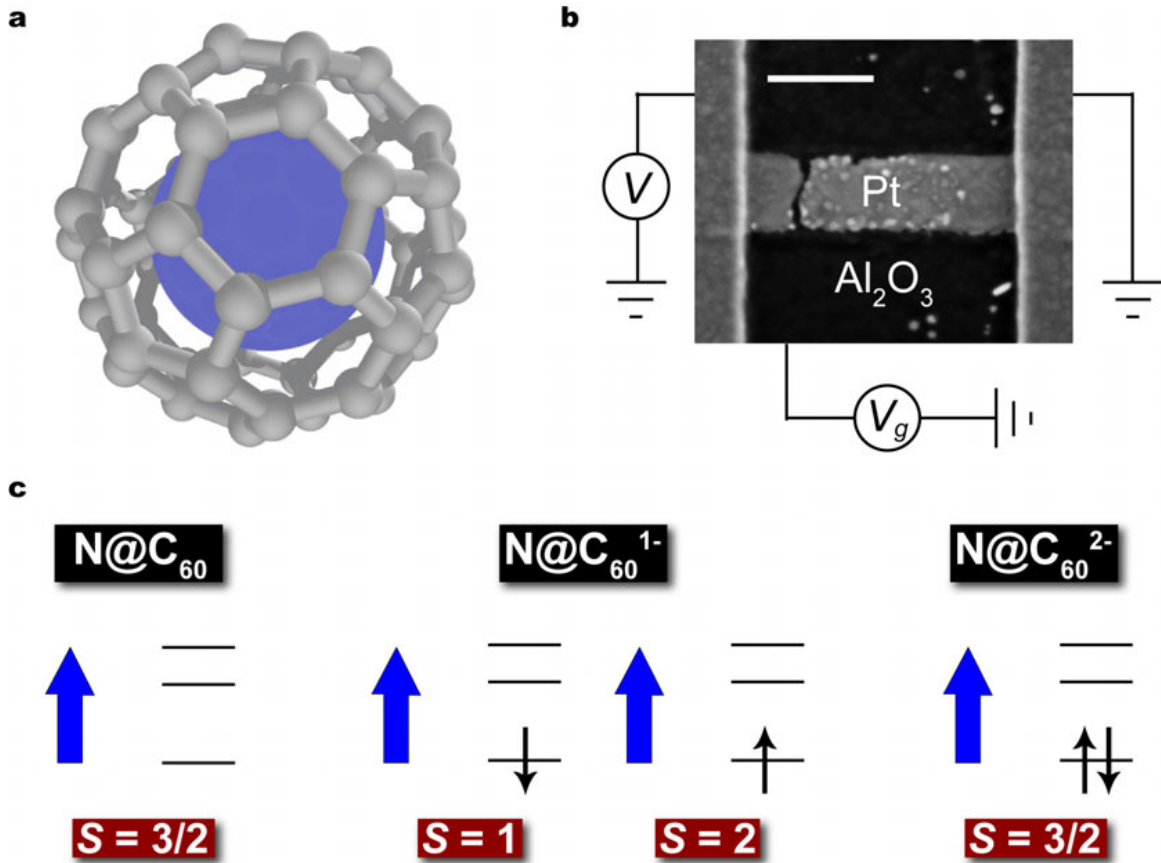


**Figure 1** Device geometry, and the spin states of N@C<sub>60</sub>. **a**, Schematic diagram of the N@C<sub>60</sub> molecule. **b**, Scanning electron microscopy image of a sample at room temperature following electromigration. The scale bar denotes 200 nm. The circuit schematic shows our biasing convention. **c**, Spin states for N@C<sub>60</sub> and its anions. The blue arrows represent the  $S_N = 3/2$  spin of the N atom. The horizontal black lines represent the lowest unoccupied molecular orbitals of the C<sub>60</sub>. The possible total spin states of the N@C<sub>60</sub> ion are indicated.

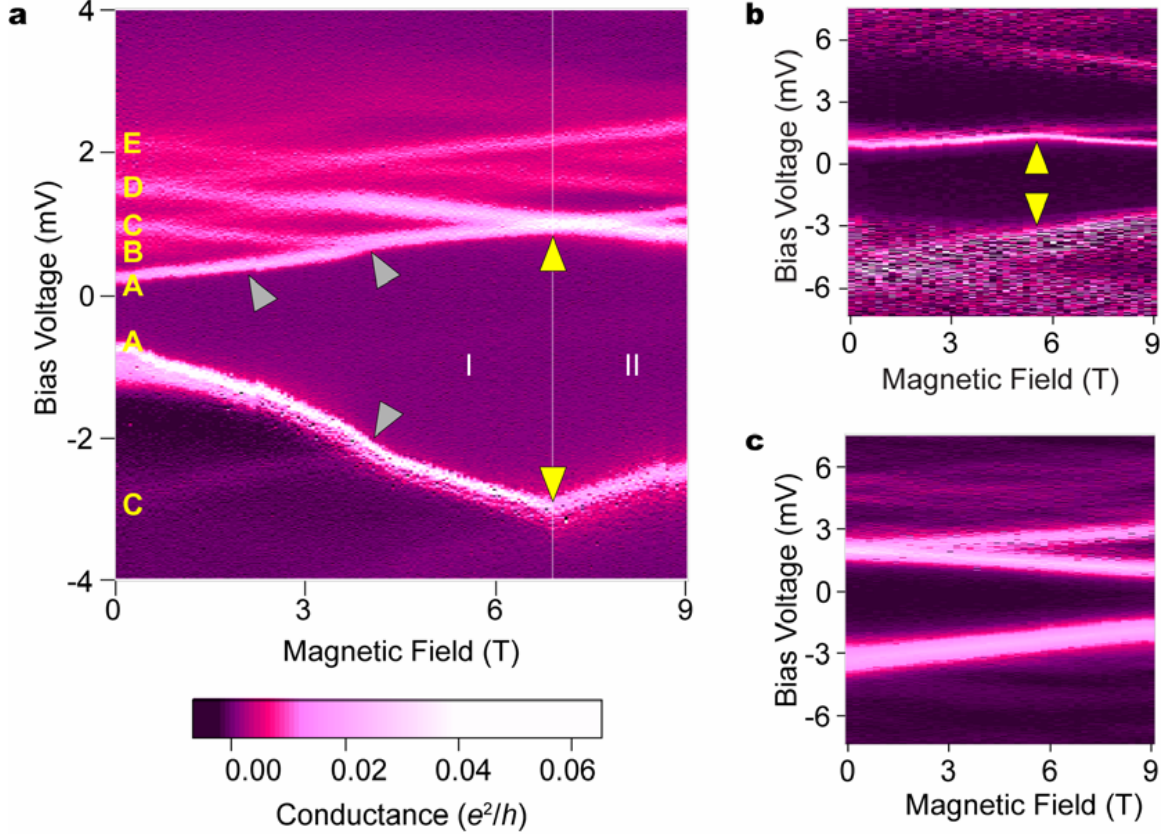


**Figure 2** Color-scale plots of differential conductance ( $dI/dV$ ) for N@C<sub>60</sub> and C<sub>60</sub> single-molecule transistors. **a**,  $dI/dV$  for N@C<sub>60</sub> device #1 as a function of source-drain voltage and applied magnetic field at constant value of gate voltage  $V_g = -891$  mV on the positive side of the degeneracy point. Yellow triangles indicate a change in slope of the ground-state peaks, and gray triangles mark the non-crossing levels discussed in the text. The labels designate different transitions. In region I, the ground-state transition corresponds to decreasing spin,  $S_{z,q+1} - S_{z,q} < 0$ , while in region II  $S_{z,q+1} - S_{z,q} > 0$ . **b**, Same as **a** for N@C<sub>60</sub> device #2. The maximum of the color scale is  $0.15 e^2/h$ . **c**,  $dI/dV$  as a function of  $V$  and  $B$  at constant  $V_g$  on the positive side of the degeneracy point for a C<sub>60</sub> single-molecule transistor. The maximum of the color scale is  $0.02 e^2/h$ . No change in slope is observed for the ground-state peaks of C<sub>60</sub>.

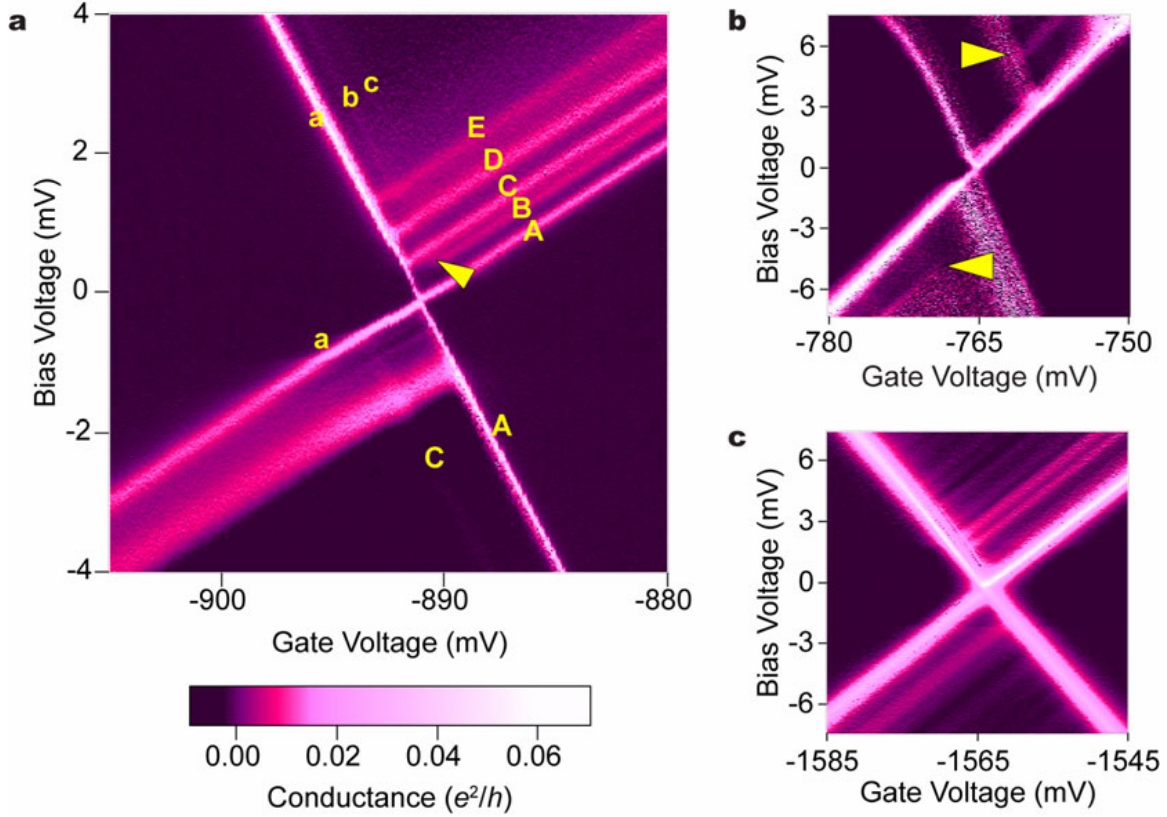


**Figure 3** Color-scale plots of differential conductance ( $dI/dV$ ) as a function of bias voltage and gate voltage at zero applied field ( $B = 0$  T). **a,b**,  $dI/dV$  from the same  $N@C_{60}$  devices #1 and #2 shown in Fig. 2a and b, respectively. The labels in **a** designate different transitions, consistent with Fig. 2a. Their energies, determined by extrapolating the transition lines to the Coulomb-blockade threshold, are ( $\pm 0.02$  meV)  $E_B - E_A = 0.29$  meV,  $E_C - E_A = 0.48$  meV,  $E_D - E_A = 0.93$  meV,  $E_E - E_A = 1.35$  meV,  $E_b - E_a = 0.20$  meV and  $E_c - E_a = 0.41$  meV. The triangles indicate the termination of ETE peaks associated with non-equilibrium excitations. **c**,  $dI/dV$  for the same  $C_{60}$  device shown in Fig. 2c. No ETE peaks are visible for this nonmagnetic molecule.

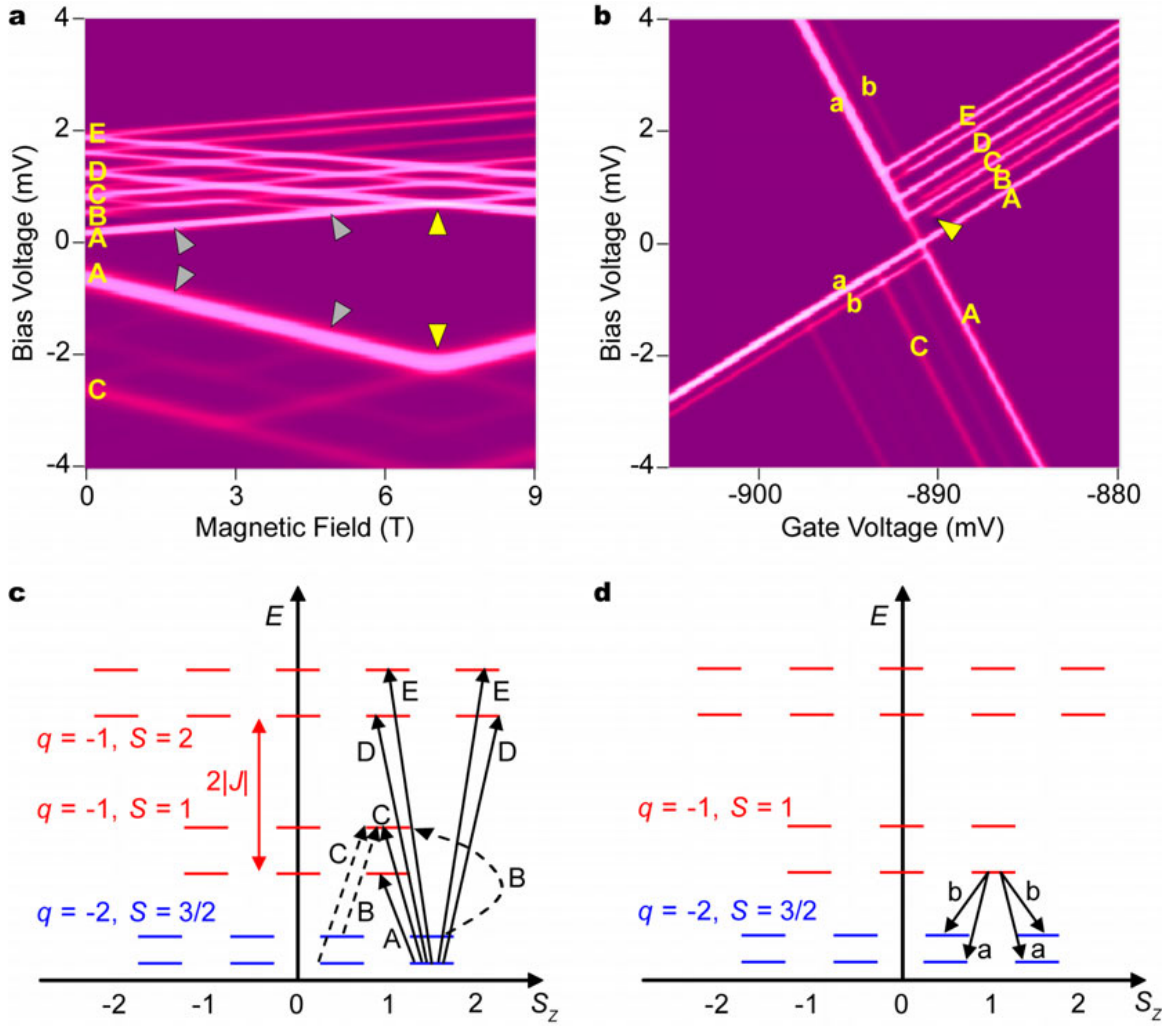


**Figure 4** Numerical calculation of the tunneling spectrum for N@C<sub>60</sub>, with parameters chosen to mimic the data for Device #1. **a**, Calculated  $dI/dV$  as a function of  $V$  and  $B$  at constant  $V_g$  on the positive side of the  $q = -2 / q = -1$  degeneracy point. Compare to Fig. 2a. The yellow triangles mark the spin-state transition, and the gray triangles mark non-crossing levels. **b**, Calculated  $dI/dV$  as a function of  $V$  and  $V_g$ . The triangle marks the termination of a nonequilibrium ETE peak. Compare to Fig. 3a. **c**, Energy level diagram at zero applied magnetic field showing examples of allowed tunneling transitions from the charge  $q = -2$  states (blue) to the  $q = -1$  states (red) of N@C<sub>60</sub>, assuming that magnetic anisotropy is negligible. The dotted lines show nonequilibrium transitions. (The dotted

line labeled C is nonequilibrium when a magnetic field is applied.) **d**, Examples of allowed tunneling transitions from  $q = -1$  states to  $q = -2$  states. The letters labeling the transitions in **c** and **d** can explain the labeled states in Figures 2a, 3a. The relative energies of the  $q = -1$  and  $q = -2$  states will depend on  $V_g$ .